JOURNAL OF GEOPHYSICAL RESEARCH, VOL. 96, NO. B10, PAGES 16,151–16,160, SEPTEMBER 10, 1991

Seafloor Compliance Observed by Long-Period Pressure and Displacement Measurements

WAYNE C. CRAWFORD, SPAHR C. WEBB, AND JOHN A. HILDEBRAND

Scripps Institution of Oceanography,
University of California, San Diego
La Jolla

Ocean surface waves with periods longer than 30 s create periodic, horizontally propagating pressure fields at the deep seafloor. Seafloor displacements resulting from these pressure fields depend on the density and elastic parameters of the oceanic crust. The displacement to pressure transfer function, the seafloor compliance, provides information about ocean crustal density and elasticity, and we outline a linearized inversion method to determine ocean crustal shear velocity from the compliance. By computing compliance partial differences with respect to changes in ocean crust shear velocity, we provide estimates of inversion stability and of the compliance sensitivity to crustal properties. Seafloor compliance, measured from pressure and acceleration spectra, is presented for two different sites: Axial Seamount on the Juan de Fuca Ridge and the West Cortez Basin in the California continental borderlands. The compliances and inverted structure for these two sites show significant differences; in particular, a zone of low shear strength is observed at depth within Axial Seamount, suggesting the presence of at least 3% partial melt within the upper 2500 meters of the ediface. These results suggest that the method provides a useful new geophysical prospecting tool.

INTRODUCTION

Knowledge of oceanic crustal structure provides important insights into crustal formation and hydrothermal circulation. Seismic methods are a practical approach to determining crustal structure; however, compressional and shear properties must be measured to provide a complete seismic picture of the oceanic crust. Shear velocities are particularly difficult to measure with conventional seismic techniques and are essential to determining oceanic crustal porosity [*Fryer et al.*, 1991]. Crustal porosity constrains hydrothermal circulation and seafloor acoustic reflectance, as well as providing information about oceanic crustal formation. A geophysical prospecting method sensitive to shear velocity structure could sense crustal magma chambers, which have low shear velocity.

We present a method for profiling ocean crustal elastic parameters using the ocean bottom pressure field as the driving source. This method is a development of a technique pioneered in shallow water by Yamamoto and others [*Yamamoto and Torii*, 1986; *Trevorrow et al.*, 1988; *Yamamoto et al.*, 1989]. A low-frequency pressure field is created on the ocean bottom by ocean surface gravity waves. The horizontal scale of the pressure field is set by the wavelength of the surface gravity waves. This pressure field causes deformation of the seafloor, resulting in seafloor pressure and vertical acceleration which show significant coherence below 0.03 Hz (Figures 1 and 2). The amplitude of seafloor deformation below 0.03 Hz depends on oceanic crustal elastic parameters, especially shear properties; low crustal rigidity leads to large seafloor displacements. Seafloor compliance is the transfer function between seafloor deformation and seafloor pressure as a function of frequency. We present measurements of seafloor compliance from two sites: Axial Seamount on the Juan de Fuca Ridge and the West Cortez Basin in the California continental borderlands. Seafloor compliance is significantly different at the two sites. West Cortez Basin has a thick sediment layer and is more compliant at high frequencies corresponding to shallow levels. Axial Seamount, an active volcano, has relatively high compliance at low frequencies corresponding to deep levels, suggesting reduced shear strength at depth within the volcano.

Coherence between seafloor pressure and vertical acceleration is also high in the microseism band, above 0.1 Hz. Energy in the microseism band is primarily associated with propagating elastic waves along the seabed and in the water. The compliance function in this band depends on phase velocities of the many modes of the oceanic waveguide. *Bradner* [1963] and others have suggested that ratios of vertical displacement to pressure associated with microseisms could be used to determine crustal structure, but in practice the various modes interfere to provide an ambiguous result.

Relating oceanic crustal structure to compliance has roots in work on Earth tides. *Beaumont and Lambert* [1972] determined that Earth tide measurements were contaminated by ocean tidal loading dependent on the structure of the Earth's upper layers. Measurements of ocean tidal loading from stations on land have proven useless for studying the elastic structure of the Earth because of the complicated tidal structure in coastal regions and the large wavelength of the effect. Measurements at the deep seafloor at tidal frequencies may be of more use for determining deep elastic structure. Recently, Yamamoto and others [*Yamamoto and Torii*, 1986; *Trevorrow et al.*, 1988; *Yamamoto et al.*, 1989] found the compliance of sediments forced by gravity water waves in shallow water (10-50 m) could be inverted to determine the shear modulus in the sediment. We invert compliance data for Earth structure using a technique applicable to hard rock as well as sediments. The inversion constrains shear velocities at sites where compressional velocities are constrained by other techniques, such as seismic refraction.

This paper differs from previous work in three areas: instrumentation, forward modeling of compliance, and inversion methods. The differences in instrumentation and forward modeling are necessary because our measurements are made at lower frequencies corresponding to the long wavelengths of ocean penetrating water waves in the deep ocean (more than 1000 m deep). We will briefly outline the theory of infragravity waves and seafloor compliance, then explain the method we use to invert

Paper number 91JB1577.
0148-0227/91/91JB-01577$05.00

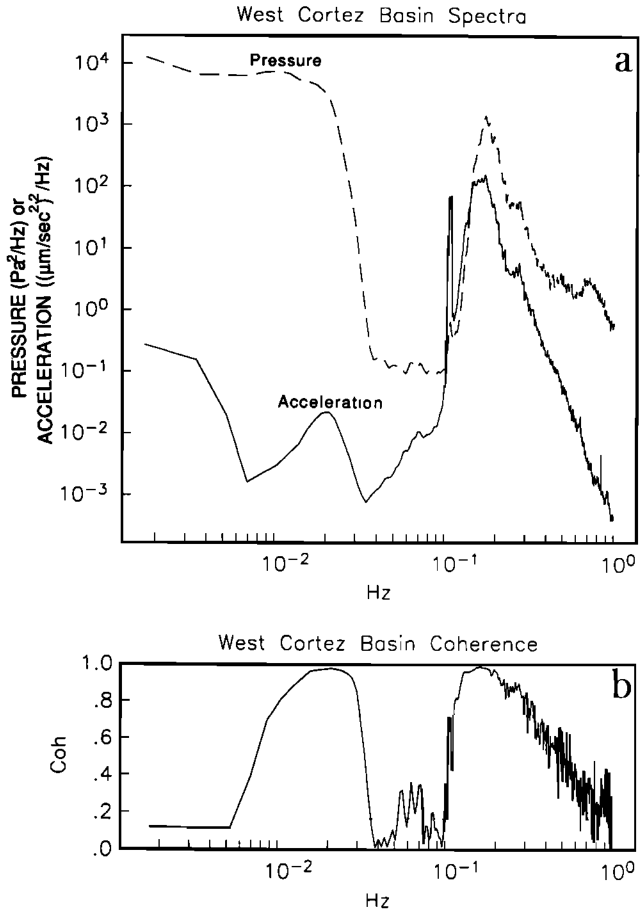

Fig. 1. West Cortez Basin (32°16'N, 119°14'W): (*a*) pressure and acceleration spectra; (*b*) coherence (solid curve) and 95% significance level (dotted line).

compliance data for shear velocity. Finally, we will show and invert compliance measurements at two oceanic sites.

THEORY

The term "infragravity wave" is used to describe long-period ocean surface gravity waves. Infragravity waves are differentiated from shorter period surface gravity waves because they are not directly generated by the action of wind on the water surface. Recent work has shown most of the long-period energy is generated at coastlines and propagates into deep water as free surface waves. The pressure field on the deep seafloor at periods greater than 20 s is generated by these waves [*Webb et al.*, 1991]. The waves have small amplitude, linear displacements, a simple frequency-to-wavenumber relation and wavelengths comparable to or greater than the ocean depth (shallow-water waves). The dispersion relation for a surface gravity wave is:

$$\omega^2 = gk \tanh(kH), \tag{1}$$

where ω is the angular frequency of the waves, k is the wavenumber, g is acceleration due to gravity, and H is water depth [*Apel*, 1987]. Depending on the amplitude of the infragravity waves at the ocean surface, the highest frequency waves that can exert pressure on the bottom are those with wavelengths between ½ and 2 times the water depth ($k = 2\pi/nH, 0.5<n<2$). The maximum frequency of infragravity wave seafloor pressure is therefore,

$$f_c = \left[\frac{g}{2\pi nH}\right]^{1/2}, \quad 0.5<n<2, \tag{2}$$

using $\tanh(2\pi/n) \approx 1, n\leq 2$. For $H = 1600$ m, the maximum frequency of infragravity wave signals is between 0.022 and 0.044 Hz.

Vertical stress from infragravity waves displaces the seafloor. The transfer function between seafloor displacement and stress, the seafloor compliance, depends on the crustal density and elastic properties. Two compliances can be calculated: the transfer function between vertical displacement and vertical stress (vertical compliance), and the transfer function between horizontal displacement and vertical stress (horizontal compliance). Horizontal stress at the ocean-crust interface is zero; this provides a boundary condition for the compliance derivation. All discussion of compliance in this paper refers to vertical compliance. If both pressure and acceleration measurements were noise-free (and if infragravity waves are the only processes to displace the ocean floor at frequencies below f_c), the compliance would be the ratio of displacement to pressure. We have collected vertical compliance data using a gravimeter (long- period seismometer) and a differential pressure gauge. The gravimeter measures acceleration rather than displacement, but acceleration is $-\omega^2$ times displacement in the frequency domain. The acceleration spectrum has noise in the infragravity wave range; noise in the pressure spectrum is small by comparison as shown by correlation between adjacent sensors. Assuming all random noise is in the

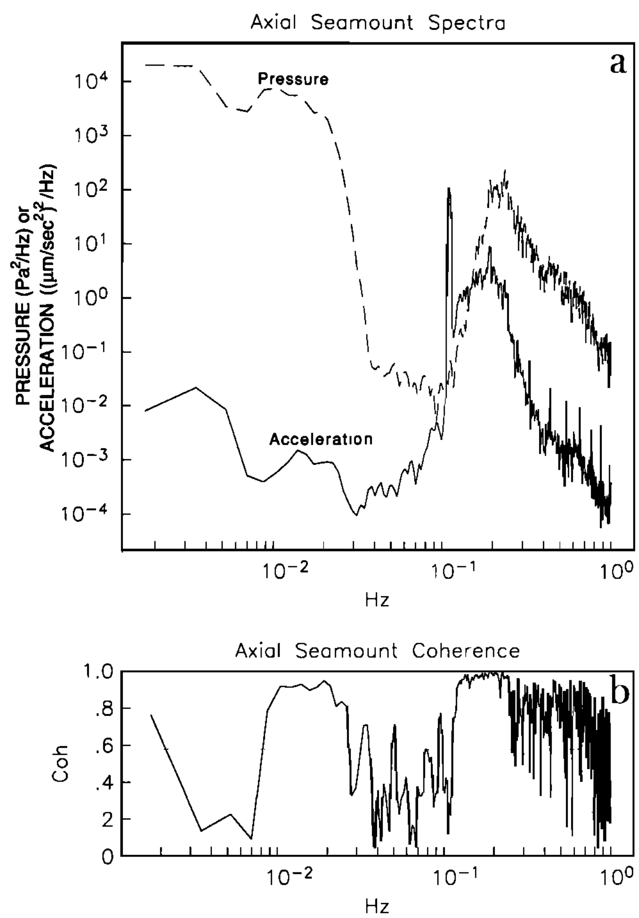

Fig. 2. Axial Seamount (45°57'N, 130°03'W): (*a*) pressure and acceleration spectra; (*b*) coherence (solid curve) and 95% significance level (dotted line).

acceleration/displacement spectrum, the square of the vertical compliance ($\hat{\xi}$) is obtained from the vertical displacement spectrum ($\hat{S}_d$), the pressure spectrum ($\hat{S}_p$), and the coherence between the two ($\hat{\gamma}_{pd}$) using the following equation:

$$\hat{\xi}^2(\omega) = \hat{\gamma}_{pd}{}^2(\omega)\,\frac{|\hat{S}_d(\omega)|}{|\hat{S}_p(\omega)|}. \tag{3}$$

Multiplying the ratio of displacement to pressure by the coherence squared accounts for both random noise in the displacement spectrum and the possibility that the low-frequency displacements have sources other than infragravity waves. An estimate of the compliance uncertainty is given by

$$\varepsilon\left[\,|\hat{\xi}(\omega)|\,\right] = \frac{\left[1-\hat{\gamma}_{pd}{}^2(\omega)\right]^{1/2}}{|\hat{\gamma}_{pd}(\omega)|\,\sqrt{2n_d}}\,|\hat{\xi}(\omega)|, \tag{4}$$

with n_d the number of data windows used to calculate the spectra and coherences [*Bendat and Piersol*, 1980].

The equation of motion in an elastic medium is:

$$\rho\frac{\partial^2 u_i}{\partial t^2} = (\lambda+\mu)\frac{\partial^2 u_j}{\partial x_j \partial x_i} + \mu\frac{\partial^2 u_i}{\partial x_j{}^2}; \tag{5}$$

u_i is the displacement of a particle in the x_i direction, ρ is the density of the material, μ is a Lamé parameter known as the rigidity or the shear modulus, and λ is the second Lamé parameter. We solve for the vertical compliance:

$$\xi(\omega) = \frac{u_z}{\tau_{zz}} = \frac{u_z}{\lambda(u_{x,x}+u_{z,z})+2\mu u_{z,z}}, \tag{6}$$

where $u_{i,j} = \partial u_i/\partial x_j$. Compressional velocity α and shear velocity β are related to the Lamé parameters λ and μ by $\rho\alpha^2 = (\lambda+2\mu)$ and $\rho\beta^2 = \mu$. Plane waves forcing the seafloor excite compressional (*P*) and vertical shear (*SV*) evanescent waves in the Earth. Equation (6) has not been solved analytically, but we can use a computational propagator matrix method to determine seafloor compliance, where the oceanic crust is modeled as a finite number of discrete flat layers overlying an infinite uniform half-space.

To relate the crustal elastic parameters and the compliance, we first model the Earth as a uniform half-space. *Sorrels and Goforth* [1973] derived the compliance of a uniform half-space when forced by a plane pressure wave traveling on the free surface at a much slower velocity than the *P* and *SV* wave velocities in the Earth. This situation is called quasi-static because the inertial terms are small, and applies to our study because infragravity waves have velocities less than 200 m s^{-1} in water up to 4000 m deep, while *P* and *SV* waves in the Earth typically travel at velocities greater than 2000 m s^{-1}. Under the quasi-static assumption,

$$\xi(\omega) = \frac{u_z}{\tau_{zz}}(\omega) \tag{7}$$

$$= -\frac{1}{k(\omega)}\left[\frac{\lambda+2\mu}{2\mu(\mu+\lambda)}\right]$$

$$= -\frac{1}{k(\omega)}\left[\frac{\alpha^2}{2\rho\beta^2(\alpha^2-\beta^2)}\right]$$

which leads to:

$$\frac{\partial|\xi|}{\partial\lambda} = -\frac{\mu^2}{2k\mu^2(\mu+\lambda)^2}, \tag{8A}$$

$$\frac{\partial|\xi|}{\partial\mu} = -\frac{2\mu^2+2\mu\lambda+\lambda^2}{2k\mu^2(\mu+\lambda)^2}. \tag{8B}$$

Since ρ, λ, and μ are always positive, all of the partial derivatives are negative; an increase in either of the Lamé parameters will result in a decrease in the magnitude of vertical compliance. The partial derivatives of $|\xi|$ with respect to seismic velocities α and β are also negative. This agrees with intuition that the less rigid or more compressible a material is, the farther it will be displaced by a given force. Assuming that different frequencies are tuned to structure at different depths in the crust, we speculate that a decrease in shear velocity at some depth will result in an increase of compliance at the corresponding frequency. From the equations (8A and 8B), $\partial|\xi|/\partial\mu$ must be at least twice the magnitude of $\partial|\xi|/\partial\lambda$ and typically is more than 5 times as great, meaning that vertical compliance is more sensitive to changes in rigidity μ than to changes in λ. Similarly, compliance is typically twice as sensitive to changes in shear velocity β than to changes in compressional velocity α. Equation (7) shows that compliance of a uniform half-space is less sensitive to changes in density ρ than to changes in compressional velocity α.

The problem of determining compliance for a laterally homogenous Earth with *P* and *SV* waves can be solved numerically. One of the most common numerical solutions is the propagator matrix method [*Aki and Richards*, 1980, pp. 273-283] combined with the method of minor vectors [*Woodhouse*, 1980]. For calculation of compliance of a known layered Earth model, we use an implementation of the minor vector propagator written by *Gomberg and Masters* [1988]. Two boundary conditions are (1) horizontal stress (τ_{zx}) vanishes at the seafloor; and (2) a uniform half-space of material underlies the layered model.

To understand the effect of crustal structure on the compliance function, we constructed five oceanic crustal models and computed their compliance, assuming a water depth of 1600 m. We

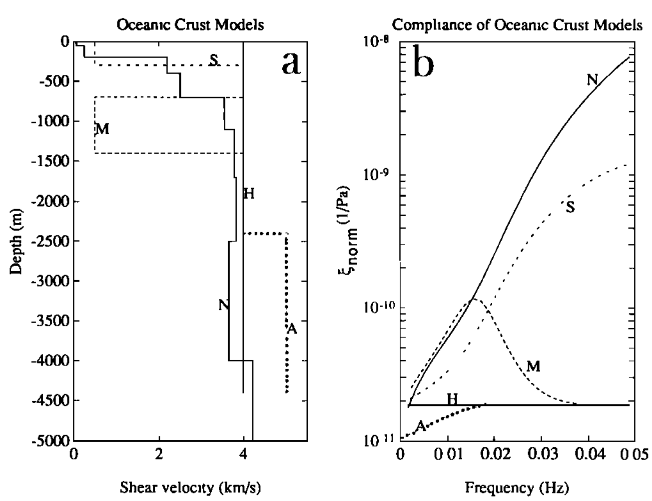

Fig. 3. Earth models and resulting compliances, H = uniform half-space, S = ideal sediment-covered model, M = ideal magma chamber model, A = ideal asthenosphere model, N = normal [*Spudich and Orcutt*, 1980] model: (*a*) shear velocities of the models: each assumes density = 2.5 g/cm^3, compressional velocity = 7 km/s; (*b*) compliances calculated from the models, assuming water depth = 1600 m, normalized by dividing by the wavenumber $k(\omega)$ of infragravity water waves.

calculate normalized compliance, the compliance after the filtering effect of the ocean is removed, by multiplying compliance by the wavenumber $k(\omega)$ of the water waves. The normalized compliance of a uniform half-space is constant (see equation (7)). Figure 3 shows the models and compliances of (1) a uniform half-space (model H); (2) a sedimentary basin model (model S); (3) a magma chamber model (model M); (4) a shallow asthenosphere model (model A); (5) normal oceanic crust [*Spudich and Orcutt*, 1980] (model N). All of the models have compressional velocity α=7 km/s, and density ρ=2.5 g/cm^3. Figure 3*b* shows that low-velocity zones correspond to regions of high compliance, in agreement with the partial derivatives of equation (8). Furthermore, it appears that shallow structure is sensed at higher frequencies than deep structure, in agreement with the intuitive argument that longer wavelength water waves penetrate deeper into the crust.

To test the properties of the compliance function inferred from Figure 3, we computed the partial differences of the compliance

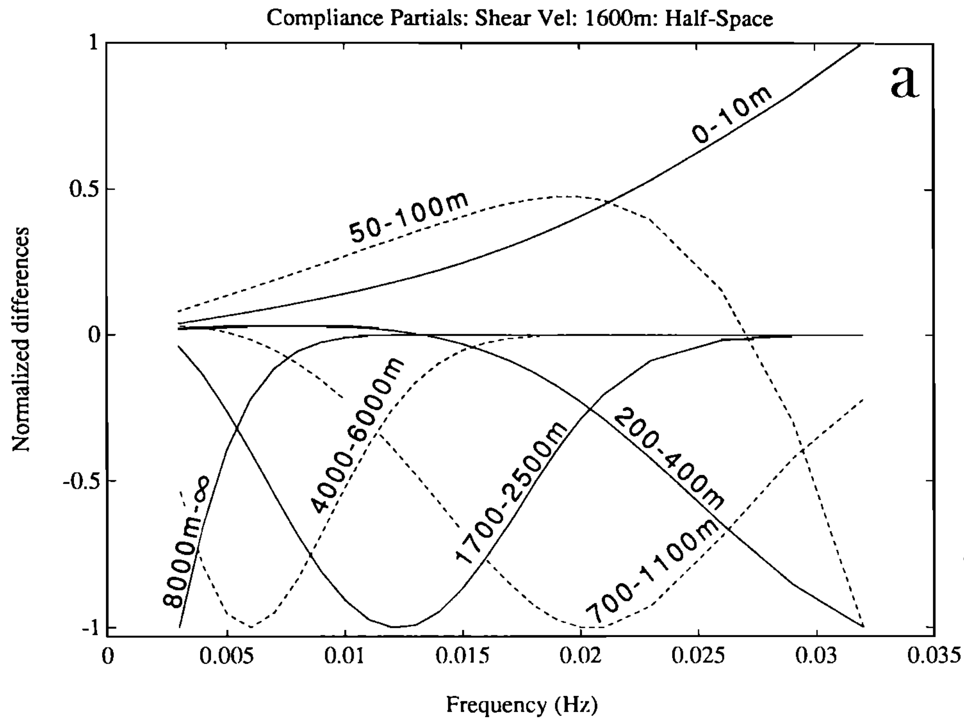

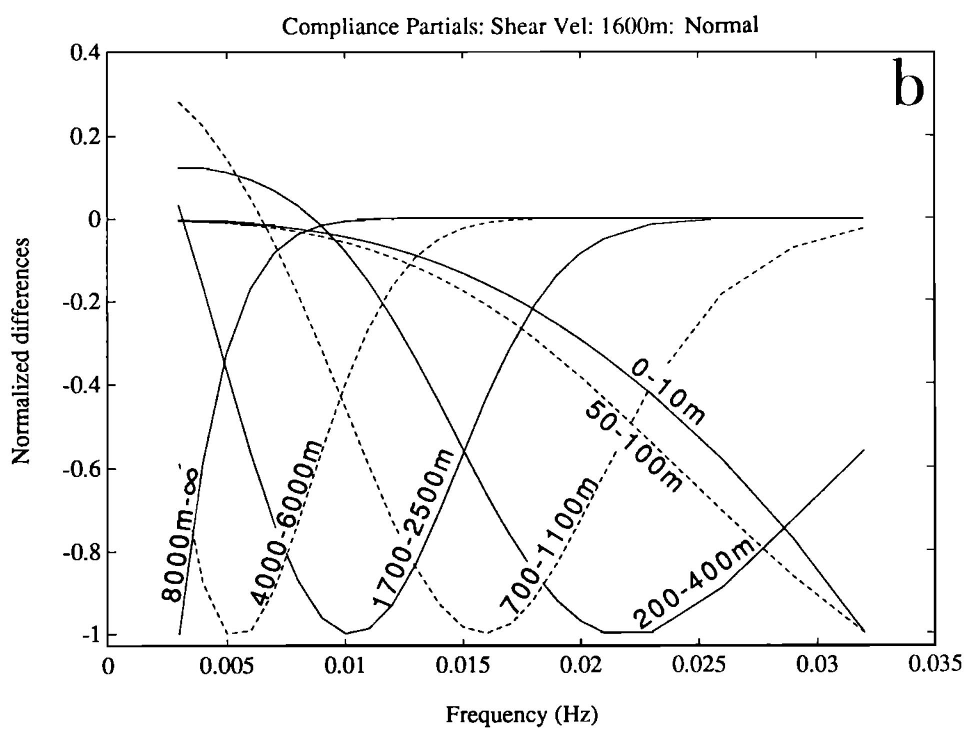

Fig. 4. Compliance sensitivity to changes in shear velocity of one layer of models H and N of figure 3. (*a*) half-space model (H) with depth of modified layer indicated, (*b*) normal oceanic crust model (N) with depth of modified layer indicated.

function for changes in shear velocity. We used the uniform half-space (model H) and the normal seafloor (model N) of Figure 3 to calculate these partial differences. To calculate each curve in Figure 4*a*, we increased the shear velocity of one layer of model H by 5% and calculated the compliance, then decreased the shear velocity of the same layer to 5% below its original value and calculated the compliance. We subtracted the second compliance from the first, and normalized the resulting vector by dividing by a positive constant so that the maximum absolute value of the vector was 1. The curves of Figure 4*b* were calculated using the same procedure, starting with the normal seafloor (model N). Normalization over emphasizes curves whose peaks are outside the frequency band of Figure 4 (the layers down to 400 m in Figure 4*a*; the layers down to 200 m in Figure 4*b*). It is apparent that different frequencies "tune" to structure at different depths, and that the tuning frequencies decrease with increasing depth. Figure 4*b*, the partials of the oceanic crust model, shows a shift of partial difference peaks to lower frequencies compared to Figure 4*a*. The low rigidity zone near the oceanic crust model surface amplifies the contribution of the shallow layers, masking the higher frequency contribution of changes in the deeper layers. If the compliance function were linear, Figures 4*a* and 4*b* would look the same. The danger of the nonlinearity is that it may allow more than one domain of attraction for the linearized compliance function. If there is more than one domain of attraction, the inversion result will not be unique. Unlike the partials calculated in equations (7) and (8), the partials of Figure 4 are not all negative. An increase in shear velocity β requires λ to decrease for the compressional velocity α to remain fixed. Therefore the effect of an increase in μ is countered by the effect of a decrease in λ. Since $\partial|\xi|/\partial\mu$ is typically greater magnitude than $\partial|\xi|/\partial\lambda$, the partial differences of compliance with respect to shear velocity are usually negative; however, $\partial|\xi|/\partial\beta(z)$ is positive at some frequencies and depths. Calculations of compliance function partial differences with respect to α and ρ suggest that compliance is typically twice as sensitive to changes in shear velocity β than to changes in compressional velocity α, and over 10 times as sensitive to changes in β than to changes in density ρ.

INVERSION

The goal of inverse theory is to calculate a model (in our case, shear velocity of the oceanic crust) from some data (in our case, seafloor compliance), when we know how to calculate the data as a function of the model. For discrete data, a discrete model, and a linear relation between the model and the data, we calculate the data vector **d** from the model vector **m** by multiplying the model by a matrix of representors **G**:

$$\mathbf{Gm} = \mathbf{d}. \tag{9}$$

Our goal is to find $\mathbf{G}^{-g}$ such that

$$\mathbf{G}^{-g}\,\mathbf{d} = \mathbf{m}^{est}, \tag{10}$$

and

$$\mathbf{Gm}^{est} = \mathbf{GG}^{-g}\,\mathbf{d} = \mathbf{d} + \mathbf{T}, \tag{11}$$

where **T** represents uncertainty in the data. If the dimension of $\mathbf{m}^{est}$ equals the dimension of **d** and **d** is exact, then $\mathbf{G}^{-g} = \mathbf{G}^{-1}$. We don't know the number and thickness of layers in the earth, however, so this calculation is unreasonable, as it will usually result in a model with more structure than is necessary to explain the data. We construct a model with many more layers than there are data points so that we will not introduce unnecessary structure into the model. Furthermore, the data are never exact. As a result, there exist an infinite number of possible $\mathbf{G}^{-g}$ and an infinite number of $\mathbf{m}^{est}$ that will fit the data equally well. To select one $\mathbf{G}^{-g}$, we must have some preconception of what a good model looks like. To force the model toward this preconception, we choose a model norm for minimization. The construction of $\mathbf{G}^{-g}$ in order to minimize the chosen norm is discussed by *Parker* [1977] and *Menke* [1984]. The most common construction methods for $\mathbf{G}^{-g}$ are to minimize the L_2 norm of the first difference or the second difference of the model (hereafter referred to as C^1L_2 and C^2L_2 inversions). These constraints are used because they attempt to make the model as featureless as possible by minimizing the slope (C^1L_2) or the curvature (C^2L_2) of the model. With the C^2L_2 constraint, structure in $\mathbf{m}^{est}$ is due to structure in the true model and not an artifact of the inversion process. Another method of construction of $\mathbf{G}^{-g}$ is the "singular value decomposition" (SVD) technique [*Menke*, 1984], which minimizes the L_2 norm of the model with the empirical property that the second difference of the model is also decreased. *Yamamoto and Torii* [1986] have successfully used the SVD method on shallow-water compliance data. We do not use the SVD method because it does not explicitly minimize the second difference of the model and therefore allows extraneous structure. Discussion and illustration of the very different models that can be obtained by different methods of inversion of discrete, inexact data are found in *Constable et al.*, [1987] and *Smith and Booker* [1988].

Linear inverse theory has developed to the point where its application is straightforward. Unfortunately, the compliance problem is nonlinear. We must write $\mathbf{G}(\cdot)$ as a function of **m**, and the linear algebra techniques of linear inverse theory are no longer applicable. A common method for solving nonlinear inverse problems is to treat them as linear inverse problems locally and to iterate to obtain a solution. This approach has the pitfall that there may be more than one "basin of attraction" for the function. The answer may not be unique, since $\mathbf{G}(\cdot)$ is dependent upon the starting model. When the problem is only weakly nonlinear (more specifically, when the functional to be minimized is convex) the linearization approach will be successful. *Yamamoto and Torii's* [1986] use of linear techniques is justified because their functional is only weakly nonlinear. We have not been able to prove that our functional is convex, so we must be more cautious in linearization of the inversion and use of techniques developed for linear inverse theory to characterize inversion quality.

We use Occam's inversion [*Constable et al.*, 1987] to obtain shear velocity structure from compliance data, using either C^1L_2 or C^2L_2 inversion. Forward problem solutions are calculated using the implementation of the minor vector propagator mentioned earlier. Models of compressional velocity ($\alpha(z)$) and density ($\rho(z)$) of the oceanic crust at the study site are assumed, and we invert compliance data for shear velocity. We use $\alpha(z)$ estimates from refraction and reflection seismology studies and estimate $\rho(z)$ based on the compressional velocities and facies analyses. Inversion accuracy is not as dependent on $\alpha(z)$ and $\rho(z)$ models as might be suspected, because of the much greater sensitivity of the compliance function to shear velocity than to these parameters.

A model with a thin layer of very low shear velocity results in a compliance function with a narrow, high compliance, peak. Relating the location of this peak to the depth of the low-velocity layer provides an estimate of the depth sensitivity of the compliance function. We calculated compliance of 28 models, each a

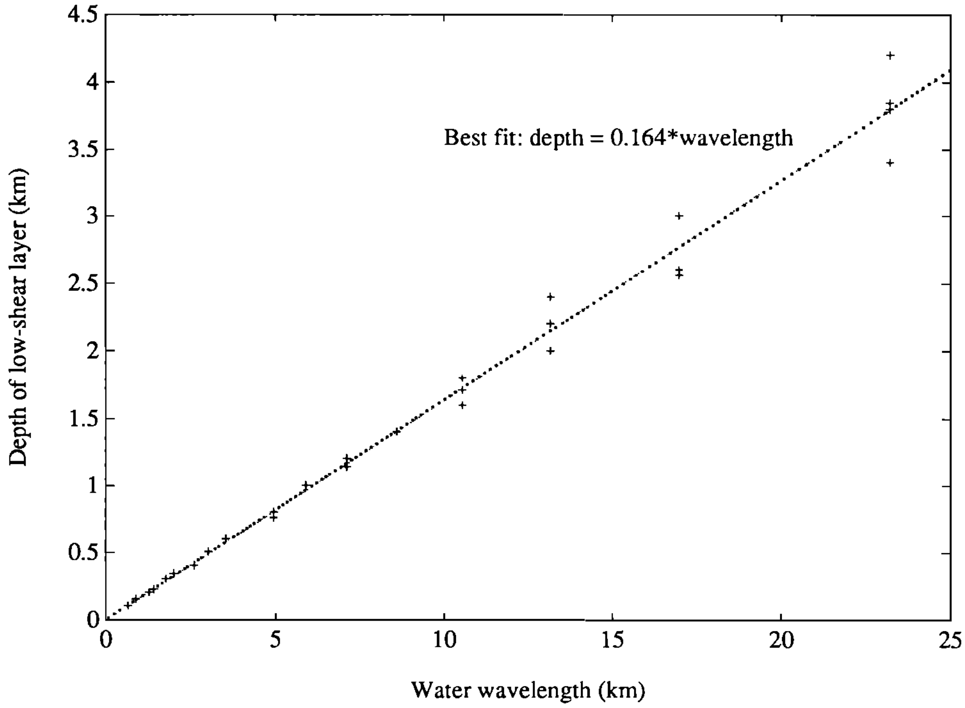

Fig. 5. Wavelength-depth relationship of a half-space with one thin layer of low shear velocity.

copy of model H with a 1 m thick low shear velocity layer inserted at a depth between 100 and 4200 m below the seafloor. We plot compliance peaks against water wavelength because the depth of penetration of water waves should depend on their wavelength. Equation (1) gives the relation between frequency and water wavelength. Figure 5 shows that the wavelength-depth relationship is linear for the uniform half-space model containing one, thin, low shear velocity layer. The water wavelengths are clustered at discrete values because they were derived from discrete frequencies. Figure 5 suggests that for the half-space model H, structural features are observed down to a depth approximately 1/6 the wavelength of the longest water wave coherent with seafloor acceleration. Because the surface waves excited in the seafloor decay exponentially with depth, the effect of seafloor structure on the compliance function decays exponentially with depth. We account for this by increasing layer thickness exponentially with depth, so that each layer has approximately equal effect on the compliance data. For the inversions in this paper we created a 50-m-thick top layer, then made every successive layer 1.1 times as thick as the layer above. The minor vector propagator program treats the bottom layer as an infinite half-space.

A standard test of linear inversion quality is calculation of a resolution matrix $\mathbf{R}=\mathbf{G}^{-g}\mathbf{G}$ [*Menke*, 1984]. For nonlinear inversion a linearized approximation of the resolution matrix is sometimes calculated from the $\mathbf{G}$ and $\mathbf{G}^{-g}$ of the last iteration of the inversion. The resulting resolution matrix often has very little to do with the actual resolution of the inversion because of the inadequacy of linearization [*Parker*, 1984]. We do not calculate resolution matrices in this paper. Instead, we computed C^2L_2 inversions of the models of Figure 3. We restricted compliance frequencies to the range obtained from our deep-ocean experimental sites. The thickness of the estimated model layers are independent of those used to generate the model, since we assumed no previous knowledge about the model. We added 5% noise to the compliances (from Figure 3*b*) before inverting.

The model inversions (Figure 6) show structure where their generating models had structure and, more importantly, no extraneous structure. Inversion of the half-space model (H) resulted in a half-space model. There is a slight error in shear velocity of the inverted half-space that is due to the 5% random noise we added to the compliances. We could easily calculate error bars for the inverted model, but only because we know that the starting model was also a half-space. Inversion of the normal oceanic crust model (N) resulted in a model very similar to model N. The negative slope below 2500 m of the N model inversion reflects a decrease in shear velocity that we put in model N at 2500 m depth. Inverted shear velocity does not increase at greater depths, suggesting that compliance in the frequency band of our experimental data cannot sense structure below approximately 2500 m depth. Inversion of the magma chamber model (M) generates a model with a low shear velocity zone, but the zone is at a greater depth than the model M magma chamber. The partial difference curves of Figure 4*b* suggest that a region of low shear velocity dominates the compliance function at lower than typical frequencies, which could be modeled as a region of slightly higher shear velocity at greater depths. The inverted model of the asthenosphere model (A) compliance data has much less structure than the original model, although it does show increasing shear velocity with depth. The inverted model's lack of structure is probably due to decreasing resolution with increasing depth, and because the structure in the asthenosphere model is near the empirical depth limit (2500 m) of the compliance frequency band. Inversion of the sediment-filled basin model (S) results in a model with more gradual velocity change than the sharp sediment-basement interface of model S. C^2L_2 inversion smooths the structure of model S over 2500 m of the inverted model. We speculate that the low shear velocity of the sediments dominate the compliance function, so that the effect of the basement rocks is not sensed until very low frequencies. We do not expect these methods will be able to discern much structure in rocks beneath a thick layer of sediments.

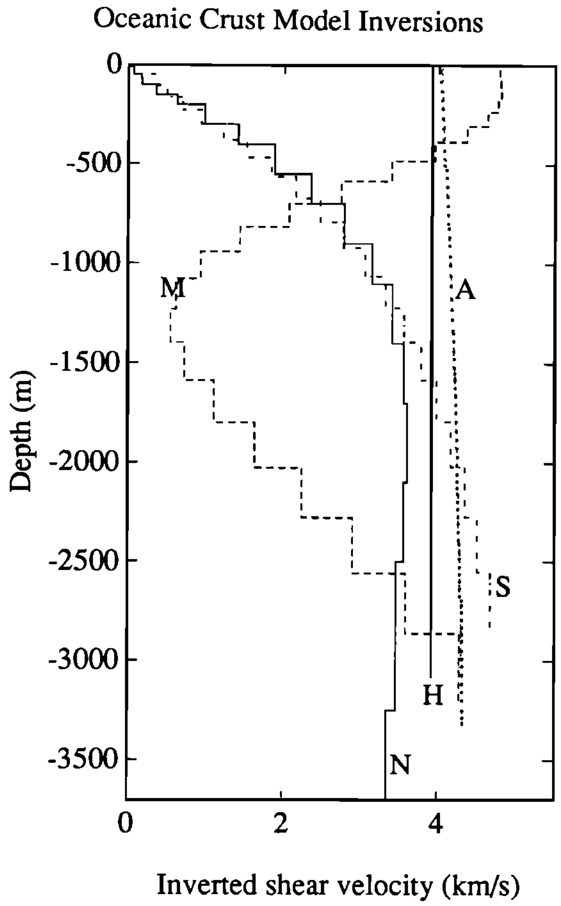

Fig. 6. Shear velocity C^2L_2 inversions of Figure 3B compliances plus 5% noise. H = uniform half-space, S = ideal sediment-covered model, M = ideal magma chamber model, A = ideal asthenosphere model, N = normal [*Spudich and Orcutt*, 1980] model.

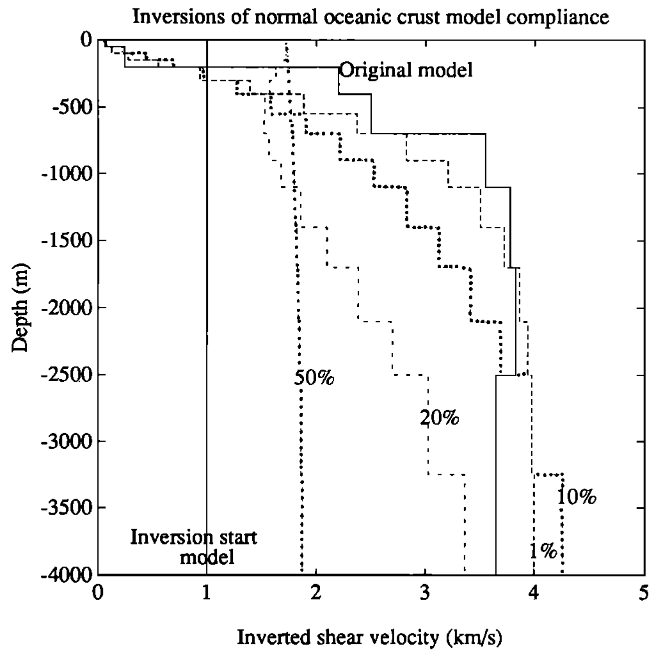

Fig. 7. Shear velocity C^2L_2 inversions of normal (model N) oceanic crust compliance plus different noise levels. Each curve is labeled with the amount of noise added to the compliance values as a percentage of the initial compliance values. Model N and the inversion starting model are displayed for comparison.

Inversion quality depends on the amount of noise in the data. Figure 7 shows inverted models of normal oceanic crust (Figure 3*a*, model N) with different noise levels added to the model's compliance. It appears that 10% noise is the most that we can accept and expect to obtain well-constrained inversions. When noise levels are high, there may be temptation to overfit the data in the model inversion. Even the slightest amount of overfitting, however, results in unwarranted and often extreme structure in the model [*Constable et al.*, 1987; *Smith and Booker*, 1988].

None of the inversions in this paper include error bars on the inverted models. When the model is an exact function of the data, it is reasonable to map uncertainty from the data onto the model. We use inverse theory because there exist an infinite number of models that fit the data equally well. The locus of these model solutions is impossible to determine, and uncertainty estimates derived from this locus would be very pessimistic estimates of the quality of our inversion, since the value of each model element is not explicitly constrained by C^2L_2 inversion. We do not ask the reader to trust the values of the model elements; instead, we state that the Earth's crust has more structure than the inverted models (compare, for example, Figures 3*a* and 5). Any structure in the inverted model reflects at least as much structure in the oceanic crust. The inference of inversion quality drawn from Figure 7 is the best quantitative error estimate we can make, and this applies only for oceanic crust models similar to model N.

INSTRUMENTATION

We use a LaCoste-Romberg underwater gravimeter to measure seafloor acceleration [*Lacoste*, 1967; *Hildebrand et al.*, 1990]. This sensor is used as a long-period seismometer on land [*Agnew and Berger*, 1978] and its useful frequency range is two decades lower than typical ocean bottom seismometers. LaCoste-Romberg underwater gravimeters are similar to conventional land gravimeters, except that the operation of underwater gravimeters is actuated by motors for leveling and for adjustment of the measurement micrometer. The sensor consists of a zero-length spring and a 0.1-kg mass. The position of the mass is sensed by capacitive plates. An analog feedback system is used to stabilize the mass position by applying a voltage to the capacitive plates. Tests of coherence between two of the land seismometers on the same pier suggest the instrument noise is flat at frequencies above 0.003 Hz, and may be as low as -181 dB relative to 1 $m^2 s^{-3}$ [*Agnew and Berger*, 1978]. The underwater gravimeter uses different electronics than these devices, however, and was limited by noise in the A/D converter at frequencies below 0.01 Hz. The gravimeter has recently been modified to reduce electronic noise; these modifications may extend the frequency range of coherence measurements and increase coherence in the infragravity wave band.

The pressure signal associated with the infragravity waves is measured using a differential gauge [*Cox et al.*, 1984]. The principle behind a differential gauge is to measure the difference of pressure between the ocean and a fluid within a rigid reference chamber. At short time scales the differences reflect pressure fluctuations in the ocean; at long time scales (greater than 1000 s) a capillary leak allows the reference chamber to equilibrate with ocean pressures. The differential mode permits the use of a very sensitive strain gauge to measure ocean pressure fluctuations while withstanding the enormous pressures of the deep ocean. Over-pressure relief valves protect the strain gauge during deployment and recovery. The gauge outperforms standard low-frequency crystal hydrophones at frequencies below 0.1 Hz. There is high coherence in the infragravity wave frequency band when the pressure gauges are placed within a few meters of each other on the seafloor, and no coherence at frequencies above the cutoff frequency f_c derived in equation (2).

The gravimeter and pressure gauge are deployed together on a deep-ocean cable from a research vessel. Data comes up the cable at 2400 baud. Each data clump contains 42 bytes, resulting in a sampling rate of 7.143 Hz. Because of the sensitivity of the spring to changes in temperature, the gravimeter is temperature stabilized by a heater coil with thermostatic feedback. Electronic coupling with the heater current created the 0.1-Hz spike evident in Figures 1*a* and 2*a*. This coupling has since been removed from the gravimeter circuitry.

MEASUREMENTS

We calculated the vertical compliance of the seafloor between 0.01 and 0.025 Hz at Axial Seamount and between 0.008 Hz and 0.034 Hz at West Cortez Basin. Coherences in these bands are significant, although the useful bandwidth is limited by noise in the acceleration spectra. We only use data for which coherences are above the 95% significance level (the dotted line in Figures 1*b* and 2*b*). Both sites are at approximately 1600 m depth. The longest water wave coherent with our seafloor acceleration data is approximately 12.5 km long (=125m/s x 100 s), corresponding to a maximum depth sensitivity of about 2.5 km.

Axial Seamount is an active submarine volcano on the Juan de Fuca Ridge. The volcanic edifice marks the intersection of the Cobb-Eikleberg hot spot trace with the Juan de Fuca Ridge. Hot spots are believed to overlie deep-seated magma sources, and oceanic ridges may contain relatively shallow magma chambers, therefore Axial Seamount is an especially promising site for location of a magma chamber. An active seismic survey of Axial Seamount by *van Heeswijk* [1986] revealed very slow shallow compressional velocities, suggesting porous shallow structure within the volcano. Van Heeswijk's survey also disclosed a possible reflector within the caldera of Axial Seamount which could be the roof of a magma chamber. The presence of a caldera at the volcano's summit further suggests that a magma chamber may exist within the edifice [*Embley et al.*, 1990]. Absolute pressure measurements by *Fox* [1990] suggest that the caldera is undergoing deflation, also consistent with the presence of a magma chamber. Our measurement site (45°57'N, 130°03'W) was in the volcano's caldera, which has no appreciable sediment cover over young volcanic flows. Compliance data were collected for 45 min at the Axial Seamount site. The 0.1-Hz heater spike in the acceleration data was removed by subtracting a least squares fit sine wave. Spectra, coherences and compliances were calculated using six segments of data, each one 4096 samples long. Each segment was multiplied by a 4π prolate-spheroidal window [*Thomson*, 1977] before application of the Fourier transform.

West Cortez Basin is a California continental borderland basin filled with up to 750 m of turbidites and hemipelagic sediments. The basin is floored by deformed Mesozoic to lower Tertiary Franciscan-type basement [*Teng and Gorsline*, 1989]. At our measurement site (32°16'N, 119°14'W) 350 m of sediments cover the basement rock, as determined by reflection seismic profiling. Compliance data were collected for 8 hours at the West Cortez Basin site. Spectra, coherences and compliances were calculated using 71 segments of data, each one 4096 samples long. Each segment was multiplied by a 4π prolate-spheroidal window before application of the Fourier transform. The West Cortez Basin data set is much longer than the data set from Axial Seamount because

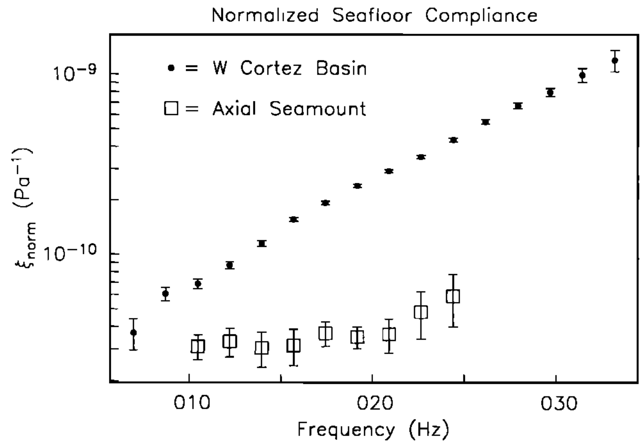

Fig. 8. Normalized compliances of Axial Seamount and West Cortez Basin calculated as in equation (3) over the infragravity wave frequency band where there is significant coherence between the two signals. Error estimates (equation (4)) are designated by vertical bars.

the instruments at the former site were deployed from a moored research platform (R/P *FLIP*) rather than a ship.

Figure 8 shows compliances calculated from the spectra and coherences of Figures 1 and 2. The effect of data series length on compliance uncertainty is evident; West Cortez Basin compliance is much better constrained than Axial Seamount compliance. C^2L_2 inversion of Axial Seamount compliance should allow less structure than C^2L_2 inversion of West Cortez Basin compliance. The West Cortez Basin compliance is significantly different than compliance at Axial Seamount. Compliances from the two sites appear to be nearly the same at the lowest frequencies but diverge at higher frequencies. Our half-space model (equations (7) and (8)) and the negative partial differences of Figure 4 predict that the low velocities of the West Cortez Basin sediments result in higher compliance at the higher-frequency end of the coherent band. Lower-frequency waves are affected by deeper structure than higher-frequency waves; waves below 0.02 Hz at West Cortez Basin are dominated by the rigid basement beneath the sediments. Error in calibration of the acceleration measurements is less than 1%. We estimate frequency-independent uncertainties in calibration of the pressure gauge to be 10%. The uncertainties are associated with the laboratory calibration, changes in electronic performance at seafloor temperatures, and compliance of pressure gauge seals. Uncertainty in the viscosity of the oil at seafloor pressures and temperatures [*Cox et al.*, 1984] affects the capillary leak time constant, creating frequency-dependent uncertainty. The time constant only affects the calibration at very low frequency; we estimate the uncertainty at 0.01 Hz to be less then 3%. The frequency-independent uncertainty of the pressure gauge calibration is relatively unimportant, because a frequency-independent change in compliance will not increase the structure of the inverted model.

Both data sets lose coherence at frequencies below 0.008 Hz (see Figures 1 and 2) due to electronic noise in the gravimeter A/D converter and decreasing acceleration signals. Gravimeter noise sources have been reduced by over 20 dB after these data were collected. The acceleration signal of a uniform half-space is proportional to ω in the infragravity wave band; we expect coherence between the gravimeter and pressure sensor will extend down to 0.002 Hz in subsequent deployments. At full ocean depth (5000 m), infragravity water waves at 0.002 Hz frequency are approximately 110 km long. Using the wavelength-depth rela-

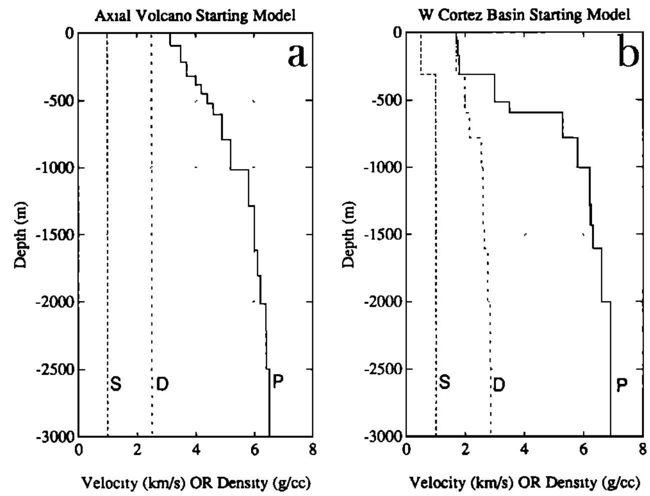

Fig. 9. Starting models for inversion of experimental data, S = shear velocity, P = compressional velocity, D = density: (*a*) Axial Seamount starting model, and (*b*) West Cortez Basin starting model.

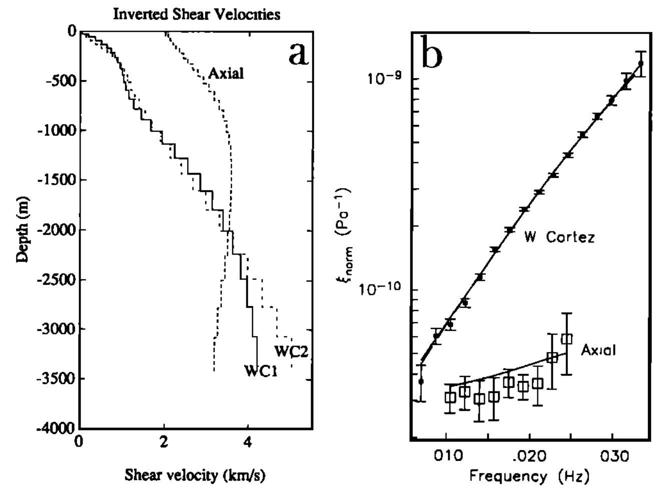

Fig. 10. Inversion of Axial Seamount and West Cortez Basin data: *a*) inverted shear velocities (WC1 = West Cortez Basin, C^1L_2 inversion; WC2 = West Cortez Basin, C^2L_2 inversion), and *b*) comparison of compliances of inverted models to data.

tion of Figure 5, compliance values taken in water of 5000 m depth may be sensitive to structure to a depth of 18 km below the seafloor. Compliance inversion is useful at ridge crests because of a lack of masking effects from sediments and because changes in shear velocity are probably more distinct near ridge crests. A typical ocean depth over a ridge crest is 2000 m; 0.002-Hz water waves have wavelengths of 70 km, and may be able to sense to 11 km depth. Deep structure is determined with lower resolution than shallow structure. Inversion of the magma chamber model (M) in Figure 6 suggests that a zone of low shear velocity shifts the effect of structure at depth to lower frequencies; a conservative prediction for inversion penetration is 6-7 km at a ridge crest.

Figure 9 shows the starting models for inversions at Axial Seamount and West Cortez Basin data. Our models of density ($\rho(z)$) and compressional velocity ($\alpha(z)$) at Axial Seamount (Figure 9*a*) are based on seismic refraction and reflection studies by *van Heeswijk* [1986]. The West Cortez Basin $\rho(z)$ and $\alpha(z)$ models (Figure 9*b*) are based on seismic reflection data (Scripps Institution of Oceanography, Geological Data Center; also Calvin Lee, personal communication, 1991), California continental borderland studies by *Teng and Gorsline* [1989], and sediment elastic parameter derivations by *Hamilton* [1980]. Figure 10 shows the results of the inversions. The West Cortez Basin data are well constrained, but inversion reveals no compelling structure. We first used C^2L_2 inversion to generate a West Cortez Basin model, (WC2 in Figure 10*a*) but because the inverted model had a low second difference we also generated a C^1L_2 inversion of the data (WC1 in Figure 10*a*). This inversion is similar to the WC2 inversion and provides confidence in the quality of the inversion. It appears that structure above 2500 m is well constrained for the West Cortez basin data. The inverted Axial Seamount model (Figure 10*a*) shows shear velocity that decreases with depth at depths greater than 1500 m beneath the seafloor. The decrease in shear velocity increases the L_2 norm of the second difference of the model. C^2L_2 inversion minimizes this value to the greatest degree allowed by the data; the region of low shear velocity is required to fit the data. At 2200 m depth, shear velocity has decreased by 8% from its maximum value. Assuming that the decrease in shear velocity is due to temperature effects, we calculate β(observed)/β(normal) ≤ 0.92. Studies of temperature effects on peridotites [*Sato et al.*, 1989] reveal this velocity variation is out of the range of temperature effects on solids and suggest partial melt. Applying relations for β(partial melt)/β(solid) from an experimental study of peridotite under 10+ kBar pressure [*Murase and Fukuyama*, 1980] and numerical models of rock independent of pressure [*Schmeling*, 1985], a region of at least 3% partial melt is required between 1500 and 2500 m depth within the edifice. This result is consistent with other suggestions of a magma chamber beneath Axial Seamount based on petrologic [*Rhodes et al.*, 1990], magnetic [*Tivey and Johnson*, 1990], gravimetric [*Hildebrand et al.*, 1990], hydrothermal [*Embley et al.*, 1990] and deformational [*Fox*, 1990] studies.

CONCLUSIONS

We have described an approach to profiling Earth structure, using pressure and displacement spectra to measure vertical compliance of the oceanic crust. Displacement information is measured using a low-frequency seismometer different from those found in conventional OBSs. We measured compliance at two sites, Axial Seamount and West Cortez Basin, and the compliance data agree with our knowledge of these sites. In particular, the difference between compliance of rocks and of thick sediments is apparent. The compliance data were inverted for a model of shear velocities. The data provide evidence for a region of partial melt beneath 1500 m depth below the caldera of Axial Seamount. The inversion accuracy is presently limited by the hardware-constrained coherence bandwidth between pressure and acceleration spectra. We believe that by decreasing electronic noise in the acceleration measurements we will improve the compliance measurements, providing good coherences to frequencies as low as 0.002 Hz.

There are many unanswered questions about the oceanic crust which could be better constrained through compliance inversions. With the ability to sense shear velocity structure to 6-7 km beneath a 2000-m-deep seabed, compliance inversion should constrain shear velocities to the bottom of young oceanic crust. The compressional information obtained from active seismic source experiments is complemented by shear information from the relatively simple process of compliance inversion.

Acknowledgments. We are indebted to V. Pavlicek, T. Deaton, and P. Hammer for development, construction and maintenance of the underwater gravimeter and differential pressure gauge. R. Parker and T. Yamamoto provided critical and insightful review of the paper. We thank S. Constable for the use of the Occam's inversion subroutines, and C. Lee for providing seismic reflection data and stacking velocities from West Cortez Basin. C. Fox and the NOAA Vents program supplied valuable ship time and encouragement. Research support was provided by the ONR Marine Geology and Geophysics program and the ONR MPL/ARL Program; we thank J. Kravitz and R. Jacobson for their encouragement and support.

REFERENCES

Agnew, D. C. and J. Berger, Vertical seismic noise at very low frequencies, *J. Geophys. Res.*, *83*, 5420-5424, 1978.

Aki, K., A. Christofferson, and E. S. Husebye, Determination of the three-dimensional seismic structure of the lithosphere, *J. Geophys. Res.*, *82*, 277-296, 1977.

Aki, K. and P. G. Richards, *Quantitative Seismology: Theory and Methods*, vol. I and II, W. H. Freeman, New York, 1980.

Apel, J. R., *Principles of Ocean Physics*, Academic, San Diego, California, 1987.

Beaumont, C. and A. Lambert, Crustal structure from surface load tilts using a finite element model, *Geophys. J.*, *39*, 203-226, 1972.

Bendat, J. S. and A. G. Piersol, *Engineering Applications of Correlation and Spectral Analysis*, John Wiley, New York, 1980.

Bradner, H., Probing sea-bottom sediments with microseismic noise, *J. Geophys. Res.*, *68*, 1788-1791, 1963.

Constable, S. C., R. L. Parker, and C. G. Constable, Occam's inversion: A practical algorithm for generating smooth models from electromagnetic sounding data, *Geophysics*, *52*, 289-300, 1987.

Cox, C. S., T. Deaton, and S. C. Webb, A deep sea differential pressure gauge, *J. Atmos. Oceanic Technol.*, *1*, 237-246, 1984.

Embley, R. W., K. M. Murphy, and C. G. Fox, High-resolution studies of the summit of axial volcano, *J. Geophys. Res.*, *95*, 12785-12872, 1990.

Fox, C. G., Evidence of active ground deformation on the mid-ocean ridge: Axial Seamount, Juan de Fuca Ridge, April-June 1988, *J. Geophys. Res.*, *95*, 12813-12822, 1990.

Fryer, G. J., D. J. Miller, and P. A. Miller, Seismic anisotropy and age-dependent structure of the upper oceanic crust, in *The Evolution of Mid-Oceanic Ridges*, edited by J. M. Sinton, pp. 1-8, AGU, Washington, D. C., 1991.

Gomberg, J. S. and T. G. Masters, Waveform modeling using locked-mode synthetic and differential seismograms: application to determination of the structure of Mexico, *Geophys. J.*, *94*, 193-218, 1988.

Hamilton, E. L., Geoacoustic modeling of the sea floor, *J. Acoust. Soc. Am.*, *68*, 1313-1340, 1980.

Hildebrand, J. A., J. M. Stevenson, P. T. C. Hammer, M. A. Zumberge, R. L. Parker, C. G. Fox, and P. J. Meis, A seafloor and sea surface gravity survey of Axial Volcano, *J. Geophys. Res.*, *95*, 12751-12763, 1990.

Lacoste, L. J. B., Measurement of grav'ty at sea and in the air, *Rev. Geophys.*, *5*, 477-526, 1967.

Menke, W., *Geophysical Data Analysis: Discrete Inverse Theory*, Academic, San Diego, California, 1984.

Murase, T. and H. Fukuyama, Structure and properties of liquids and glasses, *Year Book, Carnegie Inst. Wash.*, *79*, 307-310, 1980.

Parker, R. L., Understanding inverse theory, *Ann. Rev. Earth Planet. Sci.*, *5*, 35-64, 1977.

Parker, R. L., The inverse problem of resistivity sounding, *Geophysics*, *49*, 2143-2158, 1984.

Rhodes, J. M., C. Morgan, and R. A. Liias, Geochemistry of Axial Seamount lavas: Magmatic relation between the Cobb hotspot and the Juan de Fuca Ridge, *J. Geophys. Res.*, *95*, 12713-12733, 1990.

Sato, H., I. S. Sacks, and T. Murase, The use of laboratory velocity data for estimating temperature and partial melt fraction in the low-velocity zone: Comparison with heat flow and electrical conductivity studies, *J. Geophys. Res.*, *94*, 5689-5704, 1989.

Schmeling, H., Numerical models on the influence of partial melt on elastic, anelastic, and electric properties of rocks. Part I: elasticity and anelasticity, *Phys. Earth. Planet. Inter.*, *41*, 34-57, 1985.

Smith, J. T. and J. R. Booker, Magnetotelluric inversion for minimum structure, *Geophysics*, *53*, 1565-1576, 1988.

Sorrels, G. G. and T. T. Goforth, Low frequency Earth motion generated by slowly propagating, partially organized pressure fields, *Bull. Seismol. Soc. Am.*, *63*, 1583-1601, 1973.

Spudich, P. and J. Orcutt, A new look at the seismic velocity structure of the oceanic crust, *Rev. Geophys.*, *18*, 627-645, 1980.

Teng, L. S. and D. S. Gorsline, Late Cenozoic sedimentation in California continental borderland basins as revealed by seismic facies analysis, *Geol. Soc. Am. Bull.*, *101*, 27-41, 1989.

Thomson, D. J., Spectrum estimation techniques for characterization and development of WT4 waveguide I, *Bell Syst. Tech. J.*, *56*, 1769-1813, 1977.

Tivey, M. and H. P. Johnson, The magnetic structure of Axial Seamount, Juan de Fuca Ridge, *J. Geophys. Res.*, *95*, 12735-12750, 1990.

van Heeswijk, M., Shallow crustal structure of the caldera of Axial Seamount, Juan de Fuca Ridge, M.Sc. thesis, Oregon State Univ., 1986.

Webb, S. C., X. Zhang, and W. C. Crawford, Infragravity waves in the deep ocean, *J. Geophys. Res.*, *96*, 2723-2736, 1991.

Woodhouse, J. H., Efficient and stable methods for performing seismic calculations in stratified media, *Proc. Int. Sch. Phys. Enrico Fermi*, *78*, 127-151, 1980.

Yamamoto, T. and T. Torii, Seabed shear modulus profile inversions using surface gravity (water) wave-induced bottom waves, *Geophys. J. R. Astron. Soc.*, *85*, 413-431, 1986.

Yamamoto, T., M. V. Trevorrow, M. Badiey, and A. Turgut, Determination of the seabed porosity and shear modulus profiles using a gravity wave inversion, *Geophys. J. Int.*, *98*, 173-182, 1989.

W.C. Crawford, J.A. Hildebrand and S.C. Webb, Scripps Institution of Oceanography, 0205, University of California, San Diego, La Jolla, CA 92093-0205.

(Received October 10, 1990;
revised April 25, 1991;
accepted June 12, 1991.)